

Observational tests of x-matter models

Takeshi Chiba¹, Naoshi Sugiyama² and Takashi Nakamura³

¹*Department of Physics, University of Tokyo, Tokyo 113-0033, Japan*

²*Department of Physics, Kyoto University, Kyoto 606-8502, Japan*

³*Yukawa Institute for Theoretical Physics, Kyoto University, Kyoto 606-8502, Japan*

Accepted . Received ; in original form

ABSTRACT

We study gravitational lensing statistics, matter power spectra and the angular power spectra of the cosmic microwave background (CMB) radiation in x-matter models. We adopt an equation-of-state of x-matter which can express a wide range of matter from the pressureless dust to the cosmological constant. A new ingredient in this model is the sound speed of the x-component in addition to the equation-of-state $w_0 = p_{x0}/\rho_{x0}$. Except for the cosmological constant case, the perturbations of x-matter itself are considered. Our primary interest is in the effect of non-zero sound speed on the structure formation and the CMB spectra. It is found that there exist parameter ranges where x-matter models are consistent with all current observations. The x-matter generally leaves imprints in the CMB anisotropy and the matter power spectrum, which should be detectable in future observations.

Key words: cosmology: theory – dark matter – gravitational lensing – large-scale structure of the universe – cosmic microwave background

1 INTRODUCTION

There is growing observational evidence that the mean mass density of the universe is less than the critical density. The growth of large scale structure in cold dark matter(CDM) models requires $\Gamma = \Omega_M h = 0.25 \pm 0.05$ (Peacock & Dodds 1994) where Ω_M is the ratio of the matter energy density to the critical density and h is the Hubble parameter in units of $100 \text{km s}^{-1} \text{Mpc}^{-1}$. Recent observations of high-redshift Type Ia supernovae also indicate $\Omega_M < 1$ (Garnavich et al. 1998; Perlmutter et al. 1998; Schmidt et al. 1998; Riess et al. 1998). The observations of the age of the globular clusters $12 \pm 2 \text{Gyr}$ (Chaboyer et al. 1995) and the Hubble parameter $H_0 = 65 \pm 10 \text{km/s/Mpc}$ (Freedman 1996; Riess et al. 1996), though there might be some modifications by recent Hipparcos results (Feast & Catchpole 1997; Reid 1997), indicate $H_0 t_0 \gtrsim 0.8$ where t_0 is the age of the universe. All these observational pieces of evidence may not be explained in the framework of standard CDM model(sCDM) in which $\Omega_M = 1$. The non-zero cosmological constant (Λ CDM) may be needed to increase the age of the universe as well as to make the total energy density equal to the critical density as generically predicted by inflationary cosmology (Ostriker & Steinhardt 1995). However, as noted in Nakamura et al.(1995), at least for the age problem, the cosmological constant is not the only way to solve the problem: if $H_0 t_0 > 1$, then what is needed in general is the “matter” which violates the strong energy condition such that $\rho + 3p < 0$.

Turner and White (1997) proposed xCDM as an alternative to Λ CDM models in which a nonclustering matter of $p_x = w\rho_x$ (w being constant with $-1 < w < 0$) resides in addition to ordinary CDM so that the universe has a flat geometry. They also noted some topological defects behave like the “x-component”. However, as they admit, a component with $w < 0$ is highly unstable to growth of perturbations on small scales. Therefore they assumed xCDM to be a smooth component on small scales. This assumption is not physically reasonable because i) the notion of a smooth component is not gauge-invariant and ii) it is unphysical to ignore the response of the component to the inhomogeneities in other cosmological fluid under the equivalence principle (Caldwell et al. 1998).

Recently, we have constructed a phenomenological energy momentum tensor for “x-matter” (Chiba et al. 1997) which i) is locally stable, and ii) obeys the causality. To satisfy the local stability requirement, we have to separate the sound speed $c_s^2 \equiv p_x/\rho_x$ from the coefficient of the equation of state $w_x \equiv p_x/\rho_x$. We assume x-matter obeys the equation of state such that $p_x = w_0 \rho_{x0} + c_s^2 (\rho_x - \rho_{x0})$, where p_x , ρ_x and ρ_{x0} are the pressure, the energy density and the present energy density of

x-matter, respectively. As for a background universe, this x-matter model contains both Einstein-de Sitter ($w_0 = c_s^2 = 0$) and Λ universes ($w_0 = -1$) as a limit. A new ingredient in this model is the sound speed of the x-component in addition to the equation-of-state w_0 . Since at present we do not know how the vacuum energy interacts gravitationally (Weinberg 1989), a phenomenological approach taken here is worthwhile.

On the other hand, when we deal with perturbations of x-matter to study the structure formation in the universe, the limit of the Λ universe in which density and pressure stay constant has to be carefully taken. In this case, constant density and pressure allow the existence of only smoothed distribution from the gauge-invariance. Therefore x-matter is equivalent to the cosmological term.

In this paper, we shall make further observational tests of x-matter models as alternatives to sCDM or Λ CDM. First we consider the statistics of gravitational lensing of quasars. Then we study the evolution of density perturbations of x-matter models. Accordingly, we obtain observational quantities such as the matter power spectrum and cosmic microwave background (CMB) anisotropies. The class of cosmological models we consider are spatially flat Friedmann-Robertson-Walker(FRW) models which are generically predicted by cosmological inflation. We consider x-matter, dust matter (baryon and/or CDM) and radiation (photon and neutrino) while we do not include the cosmological constant term whose density is smoothly distributed. Similar analysis was made in xCDM models (Bloomfield Torres & Waga 1996; Silveira & Waga 1997), in scaling field model (Ferreira & Joyce 1997a; Ferreira & Joyce 1997b), the decaying lambda model (Viana & Liddle 1998) and in quintessence(QCDM) model (Caldwell et al. 1998). When our paper was at the nearly end of completion, we became aware of the recent paper by Hu (1998) where similar models were considered. In his paper, he employed very general equation of states which include our model. However, since we focus on the simple, yet rather general equation of state, we could perform thorough investigation and observational tests of the model here.

The lensing frequencies are expected to be reduced in x-matter models, since in a x-matter model the distance to an object at redshift z is smaller than the distance to the same object in Λ -dominated models. We study the lensing frequencies and set quantitative limits on the present energy density of x-matter using quasar surveys.

The height and location of the peak in the angular power spectrum of CMB depend on the matter-radiation equality and the expansion rate of the universe at the surface of last scatter. Different equation-of-states yields the different matter-radiation equality time, which would leave imprint in the peak height. Non-zero c_s affects the expansion rate of the universe, and its effect would leave the imprint in the location of the peak even if for low Ω_x .

This paper is organized as follows. In §2, we review our x-matter model. In §3, we present calculations of gravitational lensing in this model. In §4, a detailed perturbation theory in x-matter models is given and the spectra of cosmic microwave background are calculated. §5 is devoted to summary. We use the units of $c = 1$.

2 X-MATTER MODEL

In this section we review our x-matter model (Chiba et al. 1997).

x-matter possesses following nature, i.e., $w_x \equiv p_x/\rho_x < 0$ to elongate the cosmic age and $c_s^2 \equiv \delta p/\delta\rho \geq 0$ to stabilize growth of perturbations. c_s represents the sound speed of x-matter and determines how the density evolves. Together with the latter condition, we demand that it is not faster than the speed of light from the causality. As a simple form, we employ the equation of state of x-matter as

$$p_x = w_0 \rho_{x0} + c_s^2 (\rho_x - \rho_{x0}), \quad (1)$$

where the suffix 0 denotes the present value. Although w_0 and c_s are functions of ρ_x in general, to simplify the discussion we assume that they are constants. Our x-matter model includes the cosmological constant model as a special case since $p_x = -\rho_{x0}$ for $w_0 = -1$ regardless of the value of c_s^2 . However, as is mentioned in the previous section, it should be noticed that x-matter is equivalent to the cosmological term and it is no longer ‘matter’ in this limit. According to above requirements, we consider the region $-1 \leq w_0 \leq 0$, $0 \leq c_s^2 \leq 1$, and $\rho_x \geq 0$. From the requirement that the process of Big Bang Nucleosynthesis (BBN) is not appreciably disturbed by the existence of x-matter, c_s^2 is further constrained: $0 \leq c_s^2 \lesssim 0.15$ (Chiba et al. 1997).

The energy equation is

$$\frac{d\rho_x}{da} = -\frac{3}{a}(\rho_x + p_x), \quad (2)$$

where a is the scale factor. Normalising a as $a_0 = 1$, we have

$$\rho_x = \frac{\rho_{x0}}{1 + c_s^2} \left((1 + w_0) a^{-3(1+c_s^2)} + c_s^2 - w_0 \right). \quad (3)$$

Note that $w_0 = -1$ corresponds to the cosmological constant model irrespective of c_s^2 . We also note that the cosmological constant model is an asymptotic limit in our x-matter model: $p_x/\rho_x \rightarrow -1$ as $a \rightarrow \infty$. The effective scalar field potential for the x-matter model is described in Appendix A.

The Friedmann equation in a flat universe is

$$\frac{1}{H_0^2} \left(\frac{\dot{a}}{a} \right)^2 = \frac{\Omega_M}{a^3} + \frac{\Omega_r}{a^4} + \frac{\Omega_x}{1 + c_s^2} \left((1 + w_0)a^{-3(1+c_s^2)} + c_s^2 - w_0 \right), \quad (4)$$

where Ω_M , Ω_r and Ω_x are the present density parameter of matter(baryon and CDM; $\Omega_M = \Omega_B + \Omega_{CDM}$), radiation (photon and neutrino) and x -matter, respectively and over dot denotes the time derivative.

The cosmic age is given by

$$H_0 t_0 = \int_0^1 \frac{da}{a} \left(\Omega_M a^{-3} + \frac{\Omega_x}{1 + c_s^2} \left((1 + w_0)a^{-3(1+c_s^2)} + c_s^2 - w_0 \right) \right)^{-1/2}. \quad (5)$$

Here we have neglected the energy density of the radiation components since the effect of them on the cosmic age is negligible. The functional form of $H_0 t_0$ shows that it is a decreasing function of c_s^2 or w_0 . In Fig.1, the contour plots for $H_0 t_0$ in the (w_0, Ω_x) plane are shown ($\Omega_M = 1 - \Omega_x$).

3 GRAVITATIONAL LENSING

Now we consider the statistics of gravitational lensing. We compute the predicted number of gravitational lensing events taking into account the magnification bias and compare it with the observational data. Our analysis largely depends on Kochanek (1996) since our main interest is in the comparison with Λ -dominated models. Accordingly, we will neglect the dust obscuration effect considered by Malhotra et al.(1997) and the evolution effect of lensing galaxies which would weaken the constraint.

3.1 Lensing Probability

We consider a singular isothermal model for a lens mass distribution mainly for simplicity. *Hubble Space Telescope*(HST) observations show that E/S0 galaxies are effectively singular (Tremaine et al. 1994), which may support our assumption. The effect of a finite core radius is shown to be not so significant (Kochanek 1996) because a core radius increases the cross section while decreases the amplification compared to a singular isothermal model and both effects are compensated in the lensing probability. The cross section for lensing events for a singular isothermal sphere lens model is given by (Turner et al. 1984) (see Appendix B for its derivation)

$$\sigma = 16\pi^3 v^4 \left(\frac{D_{OL} D_{LS}}{D_{OS}} \right)^2, \quad (6)$$

where v is the velocity dispersion of the dark halo of a lensing galaxy, D_{OL} is the angular diameter distance to the lens, D_{OS} is the angular diameter distance to the source, and D_{LS} is the angular diameter distance between the lens and the source.

The differential probability of a lensing event is

$$\begin{aligned} d\tau &= n_0 (1 + z_L)^3 B \sigma \frac{dt}{dz_L} dz_L, \\ &= 16\pi^3 n_0 v^4 (1 + z_L)^3 B \left(\frac{D_{OL} D_{LS}}{D_{OS}} \right)^2 \frac{dt}{dz_L} dz_L, \end{aligned} \quad (7)$$

where n_0 is the present-day number density of lensing galaxies, and B is the amplification bias factor defined below. The total lensing probability is obtained by integrating Eq.(7) with respect to z_L .

The number count of galaxies is fitted by a Schechter function (Schchter 1976)

$$\phi_g(L) dL = \phi_* \left(\frac{L}{L_*} \right)^\alpha e^{-L/L_*} \frac{dL}{L_*}. \quad (8)$$

Recent Autofib survey gives $\phi_* = 0.026 \pm 0.08 h^3 \text{Mpc}^{-3}$, $\alpha = -1.09^{+0.10}_{-0.09}$ (Ellis et al. 1996). We only consider the contribution from E/S0 type galaxies. The contribution from spiral galaxies is not so important (Kochanek 1996; Fukugita & Turner 1991; Maoz & Rix 1993) because the typical velocity dispersion ($\simeq 140 \text{km/s}$) is small. The comoving number density of E/S0 galaxies n_e is $n_e = 3.5 \times 10^{-3} h^3 \text{Mpc}^{-3}$ (Heyl et al. 1997).

We assume that the velocity dispersion of the dark halo v is related to the luminosity by a “Faber-Jackson relation” of the form $v = v_*(L/L_*)^{1/\gamma}$. For a singular isothermal model, Kochanek found that $v_* = 225 \pm 10 \text{km/s}$ and $\gamma = 4.1 \pm 0.9$ (Kochanek 1994). Following Kochanek (1996), we do not consider the $(3/2)^{1/2}$ correction in the velocity dispersion since the dynamically estimated velocity dispersion of dark matter is not different from the central velocity dispersion.

As for the distance formula, we adopt the standard angular diameter distance d_A in a FRW universe in a flat universe given by

$$d_A H_0 = \frac{1}{1+z} \int_0^z du \left[\Omega_M (1+u)^3 + \frac{\Omega_x}{1+c_s^2} \left((1+w_0)(1+u)^{3(1+c_s^2)} + c_s^2 - w_0 \right) \right]^{-1/2}. \quad (9)$$

Then the angular diameter distance between the lens and the source D_{LS} is given by

$$D_{LS}H_0 = \frac{1}{1+z_S} \int_{z_L}^{z_S} du \left[\Omega_M (1+u)^3 + \frac{\Omega_x}{1+c_s^2} \left((1+w_0)(1+u)^{3(1+c_s^2)} + c_s^2 - w_0 \right) \right]^{-1/2} \quad (10)$$

The magnification bias B is an enhancement of probability that a quasar is lensed. The bias for a quasar at redshift z with apparent magnitude m_Q is written as

$$B(m_Q, z_Q) = \frac{\int dm_Q \int_{A_{min}}^{\infty} \phi_Q(m_Q + 2.5 \log A, z_Q) P(A) dA}{\int dm_Q \phi_Q(m_Q, z_Q)}, \quad (11)$$

where $\phi_Q(m_Q, z_Q)$ is the luminosity function of quasars at redshift z_Q , A_{min} is the minimum total flux amplification, and $P(A)$ is the probability distribution for a greater amplification A .

We use the Kochanek's "best model" (Kochanek 1996) as a quasar luminosity function. In this model, like Boyle, Shanks and Peterson's model (Boyle et al. 1988), the luminosity function has the form

$$\phi_Q \propto (10^{-\alpha_Q(m-m_0(z))} + 10^{-\beta_Q(m-m_0(z))})^{-1}, \quad (12)$$

where the bright-end slope α_Q and faint-end slope β_Q are constants, while the break magnitude $m_0(z)$ evolves with redshift (Kochanek 1996)

$$m_0(z) = \begin{cases} m_0 + (z - 1.0), & z < 1 \\ m_0, & 1 \leq z \leq 3 \\ m_0 - 0.7(z - 3), & z > 3. \end{cases} \quad (13)$$

Fitting this evolution model to the quasar luminosity function data in Hartwich and Schade (1990) for $z > 1$, Kochanek find that "the best model" has $\alpha_Q = 1.07 \pm 0.07$, $\beta_Q = 0.27 \pm 0.07$ and $m_0 = 18.92 \pm 0.16$ at B magnitudes. He noted that this model is no better than Wallington and Narayan model (Wallington & Narayan 1993).

For a singular isothermal sphere, the amplitude amplification $A(r)$ from a projected lens-source separation r is

$$A = 2b_{cr}/r, \quad (14)$$

where b_{cr} is the critical impact parameter given in Eq.(B6). Then $A \geq 2$ for a singular isothermal sphere. The probability of amplification is hence

$$P(A) = 8/A^3. \quad (15)$$

Putting all these pieces together, the lensing probability is finally given by

$$\begin{aligned} \tau &= \int_0^{z_Q} dz_L \frac{dt}{dz_L} (1+z_L)^3 \int_0^{\infty} \frac{dL}{L_*} n_e v_*^4 \left(\frac{L}{L_*} \right)^{\alpha} e^{-L/L_*} 16\pi^3 \left(\frac{L}{L_*} \right)^{4/\gamma} B(m_Q, z_Q) \left(\frac{D_{OL} D_{LS}}{D_{OS}} \right)^2 \\ &= F \int_0^{z_Q} dz_L \frac{dt}{H^{-1} dz_L} (1+z_L)^3 B(m_Q, z_Q) \left(\frac{D_{OL} D_{LS}}{H_0^{-1} D_{OS}} \right)^2. \end{aligned} \quad (16)$$

Here F is given by

$$F = 16\pi^3 H_0^{-3} n_e v_*^4 \Gamma(4/\gamma + \alpha + 1) = 1.6_{-0.5}^{+0.7} \times 10^{-2}, \quad (17)$$

where $\Gamma(x)$ is the gamma function. F roughly means the probability that a quasar at horizon distance is lensed by a L_* galaxy.

Fig.2 shows the optical depth in a flat universe as a function of a source redshift z_s for $\Omega_M = 0.1, 0.3, 0.5, 0.7$, respectively. Current constraint (Kochanek 1996) may be translated as $\tau(z_s)/\tau(z_s; \Omega_M = 1) \lesssim 5$. We expect that x-matter dominated models may survive the test. Next we estimate the allowed parameter regions more quantitatively.

3.2 Comparison with Observations

We fix the parameters in the quasar luminosity function (α_Q, β_Q, m_0) but allow changes of parameters in the galaxy luminosity function within their error bars. We then compare the predicted expectation number of lenses with observed one. Data are taken from HST snapshot survey (Maoz et al. 1993) and the NOT survey (Jaunsen et al. 1995). We use only quasars at $z > 1$. The total number of quasars in the sample is then 625. The sample contains 4 lensing events caused by galaxies(0142-100,1115+080,1413+117,1268+1011). Since most of the quasars in the sample do not have a B -band magnitude, we transform m_V to a B -band magnitude using $B - V = 0.2$ as suggested by Bahcall et al.(Bahcall et al. 1992). Fig.3 shows the expected number of lenses for $w_0 = -1, -0.8, -0.6, -0.4, -0.2, 0$ and $c_s^2 = 0, 0.05, 0.1, 0.15$ as a function of Ω_x . Each curve from top to bottom corresponds to $w_0 = -1, -0.8, -0.6, -0.4, -0.2, 0$. $w_0 = -1$ corresponds to the cosmological constant model irrespective of c_s^2 . The expected number increases as Ω_x increases. However, its rate decreases for increasing w_0 or c_s^2 .

We make a maximum-likelihood analysis to determine the confidence level of model parameters. The likelihood function is

$$L = \prod_{i=1}^{N_U} (1 - p_i) \prod_{j=1}^{N_L} p_j, \quad (18)$$

where N_U is the number of unlensed quasars, N_L is the number of lensed quasars, and p_i is the probability that a quasar is lensed. L is a function of three parameters (c_s^2, w_0, Ω_x) . We allow parameters c_s^2 and w_0 in the range $0 \leq c_s^2 \leq 0.15$, $-1 \leq w_0 \leq 0$, respectively. The logarithm of the ratio of the likelihood to its maximum $-2 \ln L/L_{max}$ is asymptotically distributed like a χ^2 distribution with the degrees of freedom of parameters involved (Kendall & Stuart 1973). Thus we can determine the confidence level.

Likelihood contours are plotted in Fig.4 projected onto constant c_s plane plane. Likelihood levels are, from left top to right down, 68.3%, 95%, 99%. We find that larger Ω_x is allowed as increasing w_0 . Changing c_s has little effect on likelihood contours because the effect of c_s^2 can be significant only for much higher redshift. The 95%C.L. level can be well fitted by $\Omega_x \leq 0.85 + (1 - 4c_s^2/3)(w_0 + 1)$. The constraint on the cosmological constant model ($w_0 = -1$) is less stringent than Kochanek's because of the difference in the estimated number density of E/S0 type galaxies (Ellis et al. 1996). Taking the same number density of galaxies as Kochanek's, we obtained the constraint $\lambda_0 < 0.67$ (95%C.L.) for flat models consistent with his constraint: $\lambda_0 < 0.66$ (95%C.L.).

4 PERTURBATIONS IN X-MATTER MODELS

4.1 Evolution and General Features

The gauge invariant perturbation equations for generalized fluid, i.e., x-matter are given in the Fourier space as (Kodama & Sasaki 1984)

$$\left(\frac{\Delta_x}{1 + w_x} \right)' = -kV_x + \frac{3}{1 + w_x} \frac{a'}{a} \frac{1}{\rho} \sum_{\alpha} c_{\alpha}^2 \rho_{\alpha} \Delta_{\alpha}, \quad (19)$$

and

$$V_x' = -\frac{a'}{a} (1 - 3c_s^2) V_x + c_s^2 \left(\frac{k}{1 + w_x} \Delta_x - 3 \frac{a'}{a} V \right) + k\Psi, \quad (20)$$

where Δ_x , V_x are density and velocity perturbations of x-matter, k is the wave number, c_s^2 and $w_x \equiv p_x/\rho_x$ are sound speed and pressure-density ratio of x-matter, $'$ is the derivative in terms of conformal time η , c_{α}^2 , ρ_{α} and Δ_{α} are sound speed, density, density perturbations of the α component, respectively, \sum_{α} indicates summation in terms of all components, V is total velocity perturbations and Ψ is the gravitational potential. Above density perturbations are ones relative to the total matter rest frame. We solve these equations numerically together with equations for ordinary baryonic matter, radiation (photons and neutrinos) and/or cold dark matter. The time evolutions of x-matter density fluctuations are shown in Figure 5. In this figure, we take $h = 0.5$, $\Omega_B = 0.05$, $\Omega_x = 0.95$ and $\Omega_{CDM} = 0$. For the comparison, we plotted the evolution of CDM perturbations (a dotted line).

If we set c_s^2 to be zero in order to study the dependence on w_0 , we find decay of fluctuations near the present epoch (a dashed line). It is interesting to examine what causes this turnover. In case of CDM dominated models, we can assume Ψ is constant in time, and the scale factor $a \propto \eta^2$. Therefore from equations (19) and (20), we obtain $V_x \propto \eta$ and $\Delta_x \propto \eta^2(1 + w_x)$. Accordingly, we find $\Delta_x' \propto \eta(1 + w_x)(3w_x + 1)$. Thus, we can conclude that Δ_x decays if $w_x < -1/3$ in case of CDM dominated models. This critical value $w_x = -1/3$ corresponds to the breaking of the strong energy condition. For x-matter dominated models, we numerically find a slightly larger critical value ($w_x \simeq -0.28$). It is because even for higher w_x in these models, decay of the self-gravitational potential makes perturbations difficult to grow.

When we take a non-zero value of c_s^2 , on the other hand, we find the acoustic oscillation of fluctuations of x-matter after crossing the Jeans scale. In Figure 6, the Jeans mass scales for various Ω_x and c_s^2 are shown as a function of redshift. The Jeans mass of x-matter is defined as

$$M_J = \frac{4\pi}{3} \rho_x \left(\frac{\lambda_J}{2} \right)^3, \quad (21)$$

where

$$\lambda_J = \left(\frac{\pi c_s}{G \rho_{tot}} \right)^{1/2}. \quad (22)$$

Here ρ_{tot} is the total density defined as $\rho_{tot} = \rho_x + \rho_{CDM} + \rho_B$. Solid and dashed lines denote $w_0 = -0.2$ and -0.8 , respectively. In this figure, we find that it is difficult to form the structure below galaxy scales if $c_s^2 > 10^{-8}$ when x-matter is the dominant component of the universe. However, the constraint can be loosened if we allow the time variation of c_s^2 .

To see the effect of w_0 and Jeans oscillation, the matter transfer functions are shown in Figure 7. In panel (a), we take $c_s^2 = 0$. In this panel, smaller w_0 indicates smaller amount of x-matter in past and later matter-radiation equality since we fix the present x-matter density. Therefore the location of the knee in the transfer function which corresponds to the horizon scale of the matter-radiation equality shifts to the larger scale when we take smaller w_0 . In panel (b), on the other hand, we fix w_0 to be 0 and change c_s^2 . The Jeans oscillation is seen in the transfer function even in case of $c_s^2 = 10^{-5}$.

In Figure 8, the angular power spectra of CMB anisotropies, so-called C_ℓ are shown for the same models as Figure 5. The shape of C_ℓ for the $c_s^2 = 0$ model is quite similar to the one with the cosmological constant. The peak locations and the shape on small ℓ (large scales) of this model are different from sCDM which is the fiducial CDM models with $h = 0.5$, $\Omega_0 = 1$ and $\Omega_B = 0.05$. A dent on the large scale ($\ell \sim 15$) is caused by the decay of gravitational potential just like lambda models (see e.g., Sugiyama & Silk 1994). Since the volume of the universe of the negative w_0 model is bigger than the one of the standard Einstein-de Sitter model, the peak locations shift to the smaller scales as is shown in this figure.

On the other hand, C_ℓ of the model with high c_s^2 has a quite different shape. In this model, the universe has never become purely matter dominated or radiation dominated. In other words, the gravitational potential has been decaying all the time. This decay boosts C_ℓ in the long range of ℓ 's.

One interesting feature of this figure is that the damping locations at high ℓ of all C_ℓ 's are almost the same. It is simply because recombination history is the same regardless of the equation of state since it is determined by the ratio between the number densities of photons and baryons.

4.2 Observational Constraints

Now let us make a comparison with observational data. In Figures 9 ($h = 0.5$) and 10 ($h = 0.7$), we plot the contour maps of σ_8 , which is the rms density field in a sphere of radius $8h^{-1}\text{Mpc}$ with the top hat window function, on the $w_0 - \Omega_x$ plane. Here we employ COBE 4yr normalization (Bennett et al. 1996; Bunn & White 1997). The observational value of σ_8 is $\sigma_8 = (0.52 \pm 0.04)\Omega_0^{0.52+0.13\Omega_0}$ for flat models from the analysis of the local cluster X-ray temperature function (Ecke et al. 1996). Here Ω_0 is the density parameter of total matter in case of flat Λ -models. Similar results are obtained from other analyses (White et al. 1993; Viana & Liddle 1996). While there is Ω_0 dependence in the observational value of σ_8 , we expect the dependence of σ_8 on Ω_x and w_0 is relatively weak unless $w_0 \simeq -1$ and $\Omega_x \simeq 1$.

Employing $\sigma_8 \simeq 0.6$, we plotted total matter transfer functions in Figures 11 (panels (a)-(c) for $h = 0.5$ and panels (d)-(f) for $h = 0.7$) for various c_s 's and w_0 's. In case of $c_s^2 < 10^{-5}$, transfer functions do not depend on c_s^2 since the Jeans scale is smaller than $1h^{-1}\text{Mpc}$ even at present. Therefore the shape of transfer functions is merely controlled by the matter-radiation equality epoch since the horizon scale at this epoch corresponds to the knee of the transfer function. About the normalization of perturbations, CMB anisotropies are affected by the decay of gravitational potential, which is so-called integrated Sachs-Wolfe effect. Hence one might expect different normalization factors from the same shape of the transfer function for models with different w_0 's. However, the decay of the gravitational potential caused by w_0 takes place at very late epoch even in case $w_0 \simeq -1$ as is shown in Figure 5. Therefore the integrated Sachs-Wolfe effect does not provide dominant contribution on CMB anisotropies on the COBE scale unless the universe is dominated by x-matter. Eventually we conclude that fixing σ_8 indicates fixing the matter-radiation equality and fixing the shape of the transfer function. On the other hand, we find a mild damping feature in the transfer function on small scales just like a mixed dark matter model(i.e. cold+hot dark matter) if we take $c_s^2 \geq 10^{-4}$ because of the Jeans oscillation of x-matter perturbations. In particular, it is interesting that models with $\Omega_x \simeq 0.1$, $c_s^2 = 0.15$ and $w_0 = -0.8$ fit fairly well to the observational result by Peacock and Dodds (1994) as shown in Figure 12.

In Figure 13 ($h = 0.5$ for panels (a)-(c) and $h = 0.7$ for panels (d)-(f)), we plot C_ℓ 's of models with $\sigma_8 = 0.6$. In case of $c_s^2 < 10^{-5}$, C_ℓ 's do not depend on neither c_s , w_0 nor Ω_x (see panel (a) or (d)). Comparing to the pure CDM model, however, we find higher acoustic peaks. It is because the epoch of the matter-radiation equality is the same for models with the same σ_8 . On the other hand, the equality epochs of the pure CDM models whose σ_8 are 1.2 and 1.6 for $h = 0.5$ and 0.7, respectively, are earlier than ones of x-matter models. It is well known that the later the equality epoch, the higher the peaks are (Hu et al. 1997). It is the same for panels (b) or (e). Smaller w_0 indicates smaller amount of x-matter in past and the later matter radiation equality since we fix the present x-matter density. Therefore it is shown higher peaks for smaller w_0 . In case of larger c_s^2 , on the other hand, the peak locations are shifted on smaller scales (larger ℓ) as is shown in panels (c) or (f). With larger c_s^2 , the equation-of-state of x-matter is in between radiation and matter and x-matter is a (sub)-dominant component in the universe around the matter-radiation equality epoch even for small Ω_x . This component causes the decay of the gravitational potential since only pure radiation or matter domination keeps the potential staying constant. And this decay boosts the first acoustic peak as is shown in panels (c) or (f).

In conclusion, adopting $\sigma_8 \simeq 0.6$ constrains x-matter content $\Omega_x \lesssim 0.1$ for $c_s^2 \simeq 0.1$, or if we consider the universe to be x-matter dominated, then its sound speed is constrained as $c_s^2 < 10^{-5}$ at least at the epoch of galaxy formation. Former case

can fit the observational data by Peacock-Dodds well. With high precision measurements expected from MAP^{*}(Microwave Anisotropy Probe), PLANCK[†], 2DF[‡](2 Degree Field) and SDSS[§](Sloan Digital Sky Survey), we should distinguish x-matter models from sCDM or Λ CDM.

5 SUMMARY

We have investigated the possibility that the dark matter component has the equation of state $p_x = w_0 \rho_{x0} + c_s^2 (\rho_x - \rho_{x0})$ such that $-1 \leq w_0 < -1/3$ and $0 \leq c_s^2 \lesssim 0.15$. We have studied the detailed observational consequences of x-matter models including the statistics of gravitational lensing of quasars, matter power spectrum and cosmic microwave background (CMB) anisotropies together with a comprehensive study of density perturbations of x-matter models. The gravitational lensing statistics constrains Ω_x as $\Omega_x \leq 0.85 + (1 - 4c_s^2/3)(1 + w_0)$ (95% C.L.). We have shown that introducing the sound speed of x-component has a great effect on CMB anisotropies and matter power spectrum. We find that adopting $\sigma_8 \simeq 0.6$ constrains x-matter content $\Omega_x \lesssim 0.1$ for $c_s^2 \simeq 0.1$, which can fit the observational data by Peacock-Dodds well. Alternatively, if we consider the universe to be x-matter dominated, then its sound speed is found to be constrained as $c_s^2 < 10^{-5}$ at least at the epoch of galaxy formation. Although x-matter models are consistent with all current observations, they leave imprints in the CMB anisotropy and matter power spectrum that should be detectable in future observations.

ACKNOWLEDGMENTS

We would like to thank Dr. D.Maoz for providing us with the HST Snapshot Survey data. This work was supported in part by a Grant-in-Aid for Basic Research of the Ministry of Education, Culture, and Sports Nos. 09440106(NS) and 09NP0801(TN). One of the authors (TC) was supported by JSPS Research Fellowships for Young Scientists.

REFERENCES

Bahcall J.N. et al., 1992, ApJ, **387**, 56
 Bennett C.L. et al., 1996 ApJ, **464**, L1
 Bloomfield Torres L.F., Waga I., 1996, MNRAS, **279**, 712
 Boyle B.J., Shanks T., Peterson B.A., 1988, MNRAS, **235**, 935
 Bunn, E. F. & White, M. 1997, ApJ, **480**, 6
 Caldwell R.R., Dave R., Steinhardt, P.J., 1998, Phys.Rev.Lett., **80**, 1586
 Chaboyer B., Demarque P., Kernan P.L., Krauss L.M., 1995, Science, **271**, 957
 Chiba T., Sugiyama N., Nakamura T., 1997, MNRAS, **289**, L5
 Eke V.R., Cole S., Frenk C.S., 1996, MNRAS, **282**, 263
 Ellis R., Colless M., Broadhurst T., Heyl J., Glazebrook K., 1996, MNRAS, **280**, 235
 Feast M.W., Catchpole R.M., 1997, MNRAS, **286**, L1
 Ferreira P.G., Joyce M., 1997a, Phys.Rev.Lett., **79**, 4740
 Ferreira P.G., Joyce M., 1997b, astro-ph/9711102
 Freedman W., 1996, astro-ph/9612024
 Fukugita M., Turner E.L., 1991, MNRAS, **253**, 99
 Garnavich P.M. et al., 1997, ApJ, **493**, L53
 Hartwich F.D.A., Schade D., 1990, Annu.Rev.Astron.Astrophys. **28**, 437
 Heyl J., Colless M., Ellis R., Broadhurst T., Heyl J., 1997, MNRAS, **285**, 613
 Hu W., 1998, astro-ph/9801234
 Hu W., Sugiyama N., Silk J., 1997, Nature, **386**, 37
 Jaunsen A.O. et al., 1995, Astron.Astrophys. **300**, 323
 Kendall M.G., Stuart A., 1973, The Advanced Theory of Statistics, vol.2, 3rd edition, Griffin, London
 Kochanek C.S., 1994, ApJ, **436**, 56
 Kochanek C.S., 1996, ApJ, **466**, 638
 Kodama H., Sasaki M., 1984, Prog. Theor. Phys. Suppl., **78**, 1
 Malhotra S., Rhoads J.E., Turner E.L., 1997, MNRAS, **288**, 138
 Maoz D. et al., 1993, ApJ, **409**, 28
 Maoz D., Rix H.-W., 1993, ApJ, **416**, 425
 Nakamura T., Chiba T., 1998, preprint, YITP-98-6

^{*} <http://map.gsfc.nasa.gov>

[†] <http://astro.estec.esa.nl/SA-general/Projects/Planck>

[‡] <http://meteor.anu.edu.au/~colless/2dF>

[§] <http://www.astro.princeton.edu/BBOOK>

Nakamura T., Nakao K., Chiba T., Shiromizu T., 1995, MNRAS, **276**, L41
 Ostriker J.P., Steinhardt P.J., 1995, Nature, **377**, 600
 Peacock J.A., Dodds S.J., 1994, MNRAS, **267**, 1020
 Perlmutter S. et al., 1998, Nature, **391**, 51
 Reid I.N., 1997, AJ, **114**, 161
 Riess A., Press W., Kirchner R.P., 1996, ApJ, **473**, 88
 Riess A., et al., 1998, astro-ph/9805201
 Schechter P., 1976, ApJ, **203**, 297
 Schmidt B.P., et al., 1998 astro-ph/9805200
 Silveira V., Waga I., 1997, Phys.Rev., **D56**, 4625
 Sugiyama N., Silk J., 1994, Phys.Rev.Lett., **73**, 509
 Tremaine S. et al., 1994, AJ, **107**, 634
 Turner E.L., Ostriker J.P., Gott III J.R., 1984, ApJ, **284**, 1
 Turner M.S., White M., 1997, Phys.Rev., **D56**, 4439
 Viana P.T.P., Liddle A.R., 1996, MNRAS, **281**, 323
 Viana P.T.P., Liddle A.R., 1998, Phys.Rev., **D57**, 674
 Wallington S., Narayan R., 1993, ApJ, **403**, 517
 Weinberg S., 1989, Rev.Mod.Phys. **61**, 1
 White S.D.M., Efstathiou G., Frenk C.S., 1993, MNRAS, **262**, 1023

APPENDIX A: EFFECTIVE POTENTIAL FOR X-MATTER MODEL

We can construct the effective potential of a scalar field for the x-matter model. The method of the construction is similar to that given in Nakamura & Chiba(1998).

We consider a scalar field ϕ minimally coupled to gravity. Then the energy density and the pressure of x-matter are given in terms of the scalar field as

$$\rho_x = \frac{1}{2}\dot{\phi}^2 - V(\phi), \quad (A1)$$

$$p_x = \frac{1}{2}\dot{\phi}^2 + V(\phi), \quad (A2)$$

where $V(\phi)$ is the potential of the scalar field. By the use of Eq.(3) and Eq.(1), the scalar field and the potential can be written in terms of the scale factor

$$2V(a) = \rho_x - p_x = \frac{2(c_s^2 - w_0)}{1 + c_s^2} \rho_{x0} + \frac{(1 - c_s^2)(1 + w_0)}{1 + c_s^2} \rho_{x0} a^{-3(1+c_s^2)}, \quad (A3)$$

$$\dot{\phi}^2 = \left(aH \frac{d\phi}{da} \right)^2 = (1 + w_0) \rho_{x0} a^{-3(1+c_s^2)}. \quad (A4)$$

ϕ is given by the integral

$$\phi(a) - \phi_0 = \pm \int_1^a \sqrt{\frac{3(1 + c_s^2)(1 + w_0)}{8\pi G (1 + w_0 + (c_s^2 - w_0)u^{3(1+c_s^2)})}} \frac{du}{u}. \quad (A5)$$

Then V is given implicitly as a function of ϕ . The shapes of $V(\phi)$ for $c_s^2 = 0.0, 0.1$ are shown in Fig.14 from $a = 1$ to $a = 10^{-3}$. The scale is arbitrary. Since $V(\phi)$ involves a tiny (but positive finite) constant term, the universe will be dominated by this constant term and behave like the cosmological constant dominated universe in future.

APPENDIX B: FORMULAE FOR A SINGULAR ISOTHERMAL SPHERE LENS

Here we give useful formulae for a singular isothermal sphere lens which are necessary in the text.

The deflection angle α by an isothermal sphere lens is given by

$$\alpha = \frac{4GM(\leq b)}{b}. \quad (B1)$$

Here b is the impact parameter and $M(\leq b)$ is the mass projected within the impact parameter b

$$M(\leq b) = 2\pi \int_0^b \Sigma(r) r dr. \quad (B2)$$

$\Sigma(r)$ is the surface density and is written for a singular isothermal sphere in terms of the velocity dispersion v as

$$\Sigma(r) = \frac{v^2}{2Gr}. \quad (B3)$$

Therefore the deflection angle is written as

$$\alpha = 4\pi v^2. \quad (\text{B4})$$

The lens equation is then

$$\phi = \theta - 4\pi v^2 \frac{D_{LS}}{D_{OS}}, \quad (\text{B5})$$

where ϕ and θ are the angular position of the source and the image, respectively. The critical impact parameter is thus

$$b_{cr} = 4\pi v^2 \frac{D_{OL} D_{LS}}{D_{OS}}. \quad (\text{B6})$$

Therefore, the cross section is given by

$$\sigma = \pi b_{cr}^2 = 16\pi^3 v^4 \left(\frac{D_{OL} D_{LS}}{D_{OS}} \right)^2. \quad (\text{B7})$$

If the alignment is close enough such that $\phi \leq \alpha \frac{D_{LS}}{D_{OS}}$, lensing produces multiple images at

$$\theta^\pm = \phi \pm \alpha \frac{D_{LS}}{D_{OS}}, \quad (\text{B8})$$

An amplification due to lensing is given by

$$A = \left| \frac{\theta d\theta}{\phi d\phi} \right|. \quad (\text{B9})$$

The two images are amplified by factors

$$A^\pm = \frac{\alpha D_{LS}}{\phi D_{OS}} \pm 1. \quad (\text{B10})$$

This gives a total amplification

$$A = 2 \frac{\alpha D_{LS}}{\phi D_{OS}}. \quad (\text{B11})$$

This means that the probability distribution of total amplification for multiply imaged systems is

$$P(A)dA = 8A^{-3}dA, \quad \text{for } A \geq 2. \quad (\text{B12})$$

This paper has been produced using the Royal Astronomical Society/Blackwell Science L^AT_EX style file.

FIGURE CAPTIONS

Figure 1: The contour plots for $H_0 t_0$ in the (w_0, Ω_x) plane. The contour levels are $H_0 t_0 = 1.0, 0.9, 0.8, 0.7, 0.6$ (only for $c_s^2 = 0.15$) from top-left to right.

Figure 2: The lens optical depth for a source at redshift z_s in a flat universe relative to that in the Einstein-de Sitter model ($\Omega_M = 1$) for (a) $\Omega_M = 0.1$, (b) $\Omega_M = 0.3$, (c) $\Omega_M = 0.5$, and (d) $\Omega_M = 0.7$. Solid curves correspond to $c_s^2 = 0$, dotted ones $c_s^2 = 0.1$. Each type of curves from top to bottom corresponds to $w_0 = -1, -0.8, -0.6, -0.4$. Note that $w_0 = -1$ corresponds to the cosmological constant model irrespective of c_s^2 .

Figure 3: The expected number of lenses for $c_s^2 = 0$ (a), 0.05 (b), 0.1 (c), 0.15 (d) and $w_0 = -1, -0.8, -0.6, -0.4, -0.2, 0$ as a function of Ω_x . Each curve from top to bottom corresponds to $w_0 = -1, -0.8, -0.6, -0.4, -0.2, 0$. $w_0 = -1$ corresponds to the cosmological constant model irrespective of c_s^2 . Data is taken from HST snapshot survey (Maoz et al. 1993).

Figure 4: Likelihood contours for flat cosmological models projected onto constant c_s plane. Likelihood levels are, from left top to right down, 68.3%, 95%, 99%.

Figure 5: Time evolution of x -matter density fluctuations Δ_x at the wave number $k = 0.1 \text{ Mpc}$ for different values of w_0 and c_s^2 . Solid and dotted lines are for $w_0 = -0.8$, $c_s^2 = 0.2$ and $w_0 = -0.8$, $c_s^2 = 0$, respectively. A dashed line corresponds to the standard CDM model, i.e., $w_0 = 0$ and $c_s^2 = 0$. We take $\Omega_x = 0.95$ and $\Omega_B = 0.05$ as cosmological model parameters.

Figure 6: Jeans scale as a function of redshift. Solid lines correspond to $w_0 = -0.2$, while dashed lines to $w_0 = -0.8$.

Figure 7: Total matter transfer functions. We take $\Omega_x = 0.95$ and $\Omega_B = 0.05$ as cosmological model parameters. (a):

changing w_0 with $c_s^2 = 0$. From left to right, $w_0 = -0.8, -0.6, -0.4$ and -0.2 . Dashed and dotted lines are CDM models with the shape parameter $\Gamma = 0.5$ and 0.25 , respectively. (b): changing c_s^2 with $w_0 = 0$. From left to right, $c_s^2 = 0.15, 0.05, 10^{-4}$ and 10^{-5} .

Figure 8: CMB angular power spectra. Models are same as Figure 5.

Figure 9: Contours of σ_8 in the $w_0 - \Omega_x$ plane for various values of c_s . COBE 4yr normalization is employed. We take $h = 0.5$ and $\Omega_B = 0.05$. From top to bottom in each panels, $\sigma_8 = 0.2, 0.4, 0.6, 0.8$ and 1.0 (bold).

Figure 10: Same as Figure 9 but $h = 0.7$ and $\Omega_B = 0.04$.

Figure 11: Total matter transfer functions for models with $\sigma_8 = 0.6$. Panels (a)-(c) are models with $h = 0.5$ and $\Omega_B = 0.05$ and Panels (d)-(f) are with $h = 0.7$ and $\Omega_B = 0.04$. Solid lines are indicated in each panels. Dashed and dotted lines are CDM models with the shape parameter $\Gamma = 0.5$ and 0.25 , respectively. Since the transfer functions of the model with $w_0 = 0$ and $\Omega_x = 0.025$ and the one with $w_0 = -0.5$ and $\Omega_x = 0.04$ are identical in panel (c), we do not plot the later one.

Figure 12: Matter power spectra for ‘best fitted’ models. From Figure 11, we chose models with transfer functions similar to the ones of $\Gamma = 0.25$. (a): models with $h = 0.5$ and $\Omega_B = 0.05$. Solid and dashed lines are models with $w_0 = -0.8$ and $\Omega_x = 0.09$ and $w_0 = 0$ and $\Omega_x = 0.025$. (b): models with $h = 0.7$ and $\Omega_B = 0.04$. Solid, dotted and dashed lines are models with $w_0 = -0.8$ and $\Omega_x = 0.12$, $w_0 = -0.5$, $\Omega_x = 0.06$ and $w_0 = 0$ and $\Omega_x = 0.03$, respectively. The symbols denote the observational data by Peacock and Dodds(1994). We multiply 0.8 to these observational values since we are only interested in the shape of the matter power spectrum and Peacock and Dodds’ data provide roughly 10 – 20% larger σ_8 compared to the value quoted in the text.

Figure 13: CMB angular power spectra for models with $\sigma_8 = 0.6$. Models are same as Figure 11. Dotted lines are C_ℓ ’s of CDM models. Namely CDM models with $\Omega_0 = 1, h = 0.5$ and $\Omega_B = 0.05$ for panels (a)-(c), and with $\Omega_0 = 1, h = 0.7$ and $\Omega_B = 0.04$ for panels (d)-(f).

Figure 14: The effective scalar field potential for x-matter model with $c_s^2 = 0, 0.1$ and $w_0 = -0.8$. Scales are arbitrary.

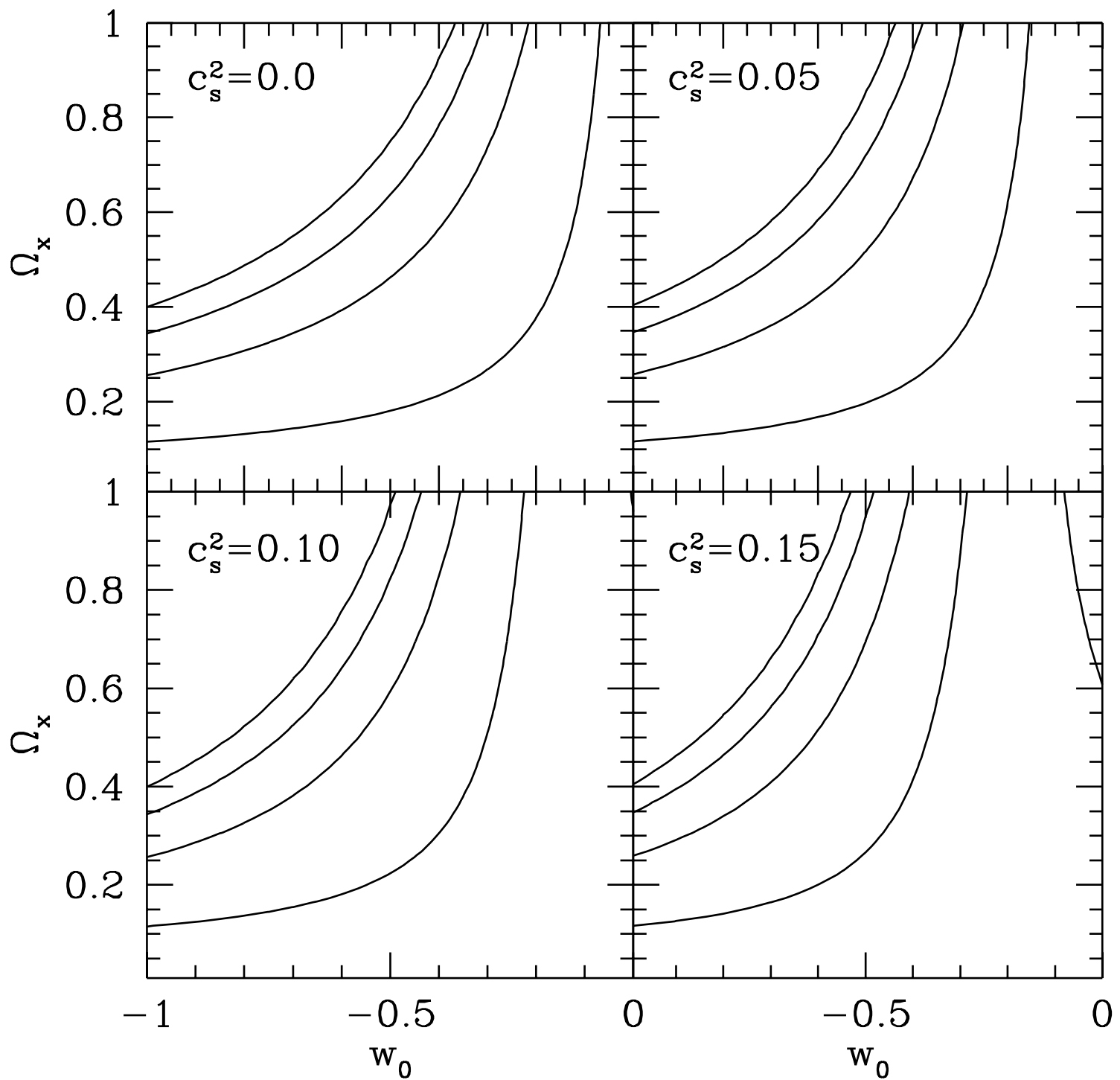


Fig. 1

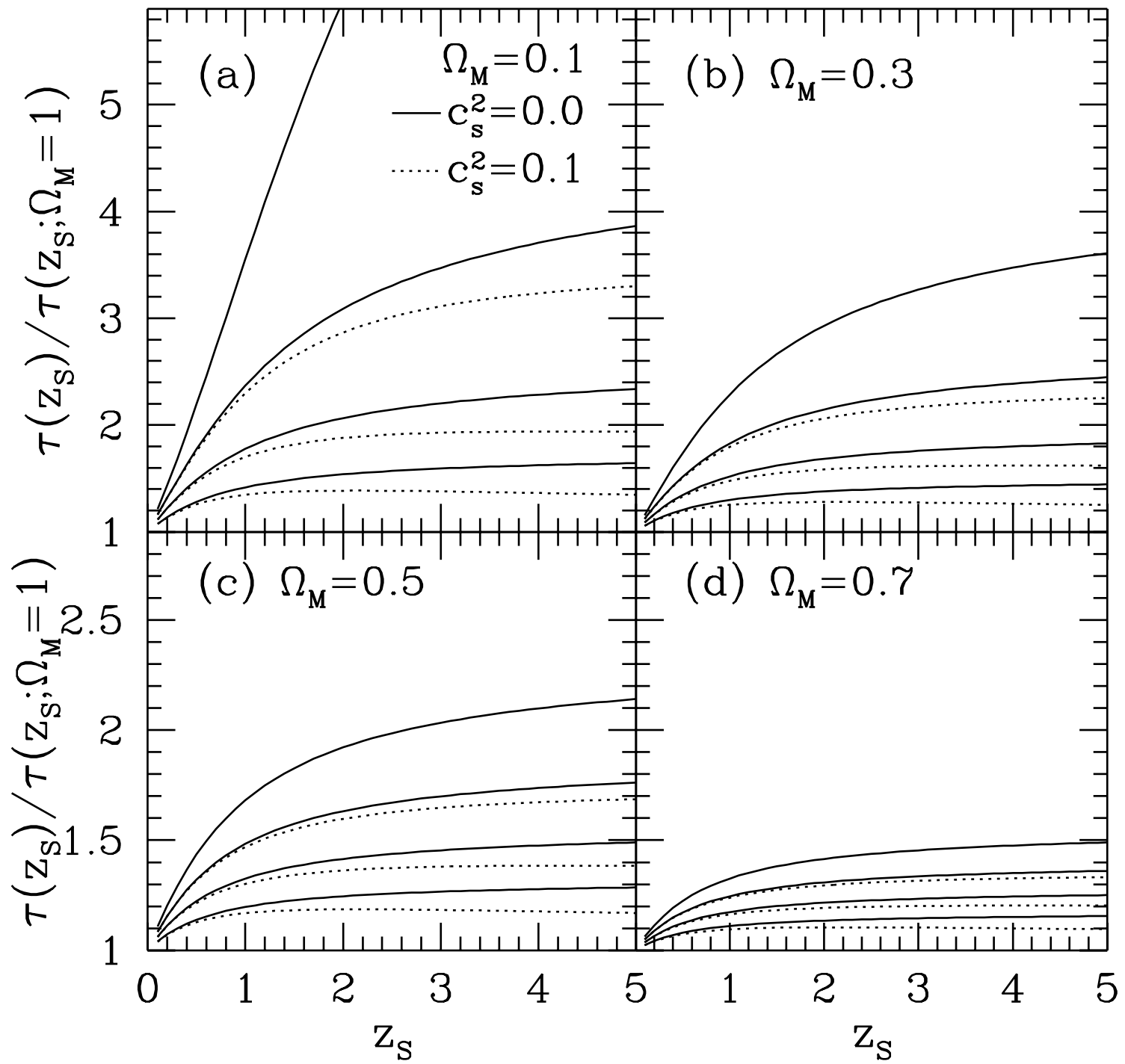


Fig. 2

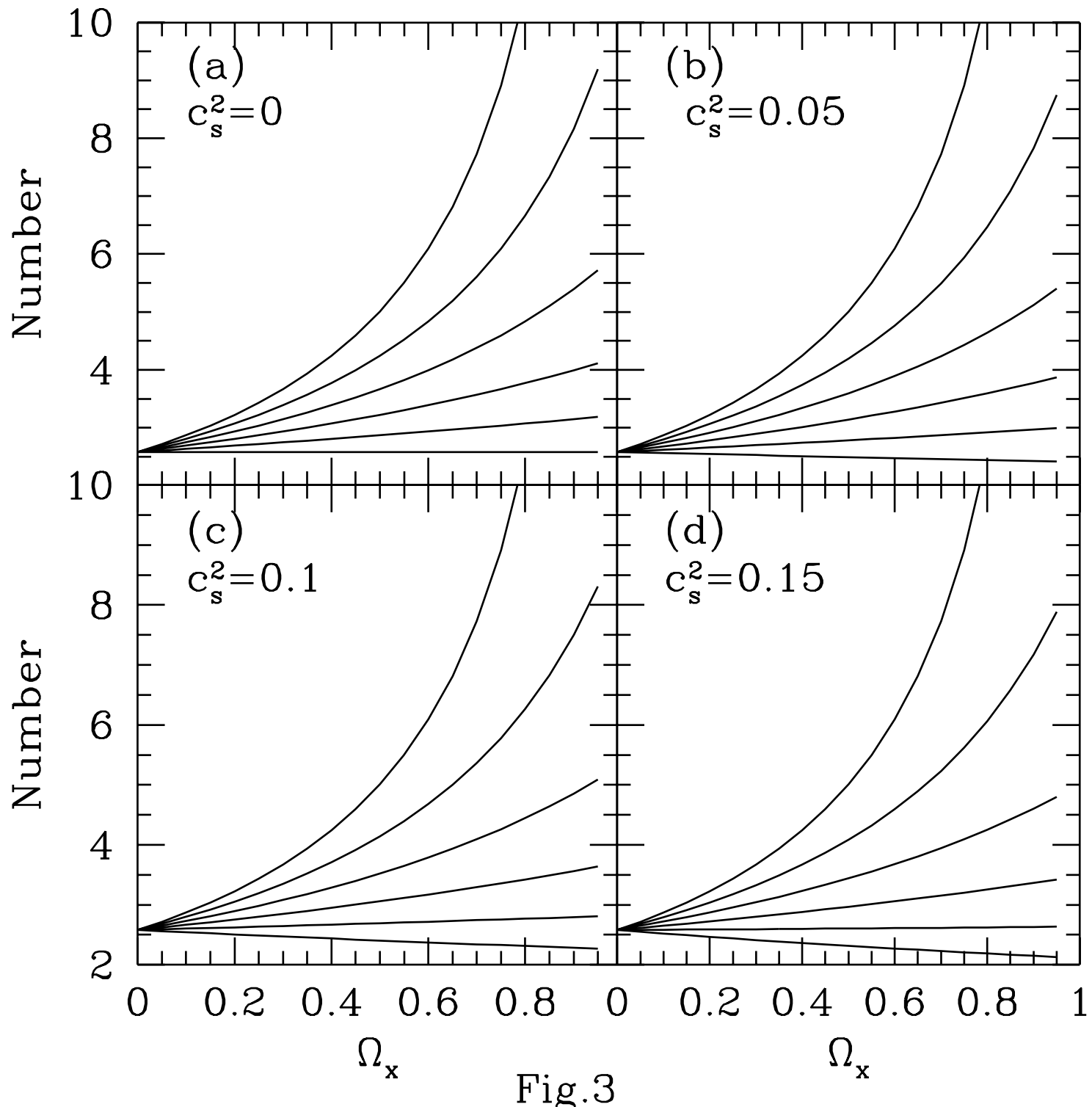


Fig.3

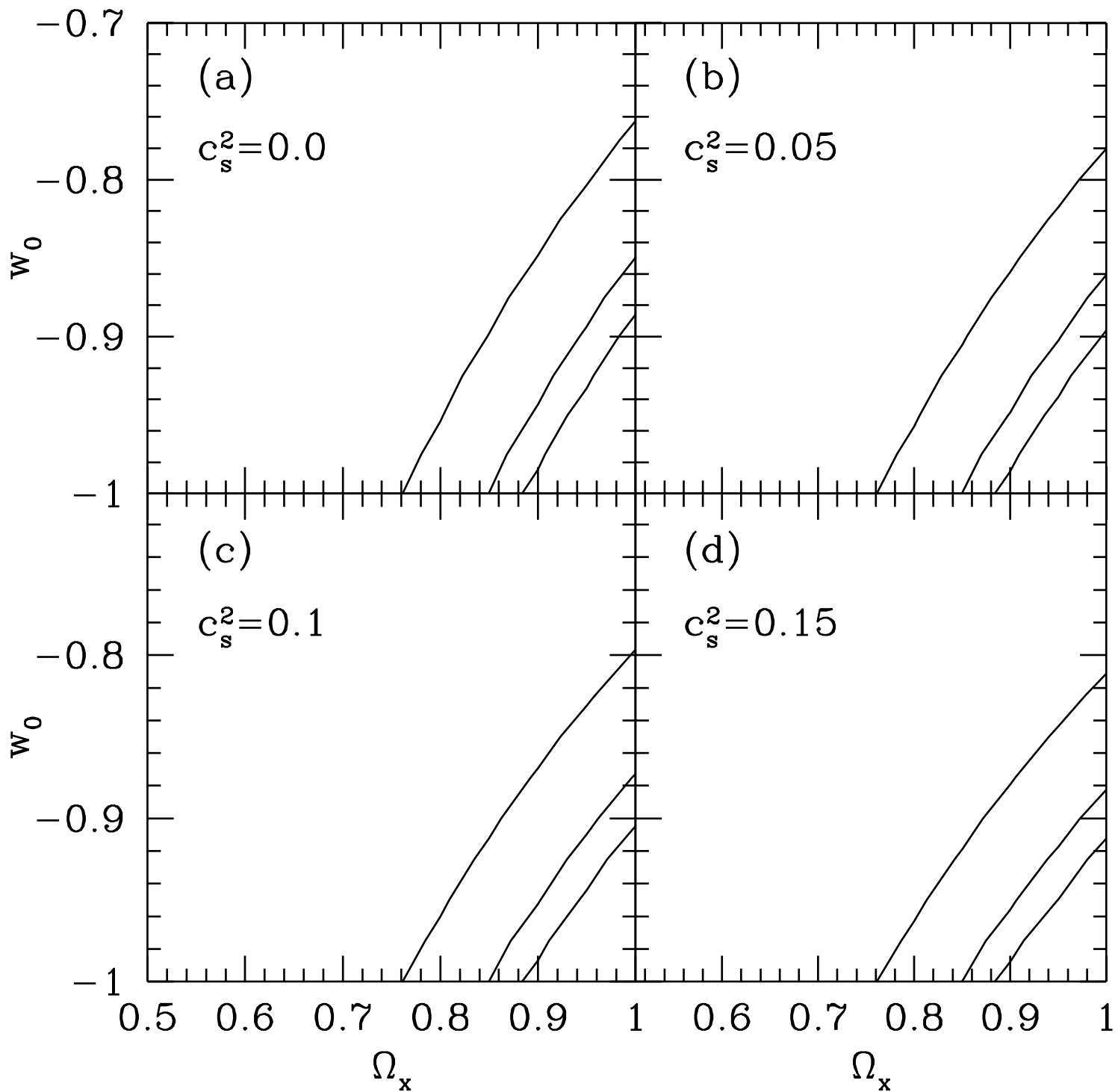
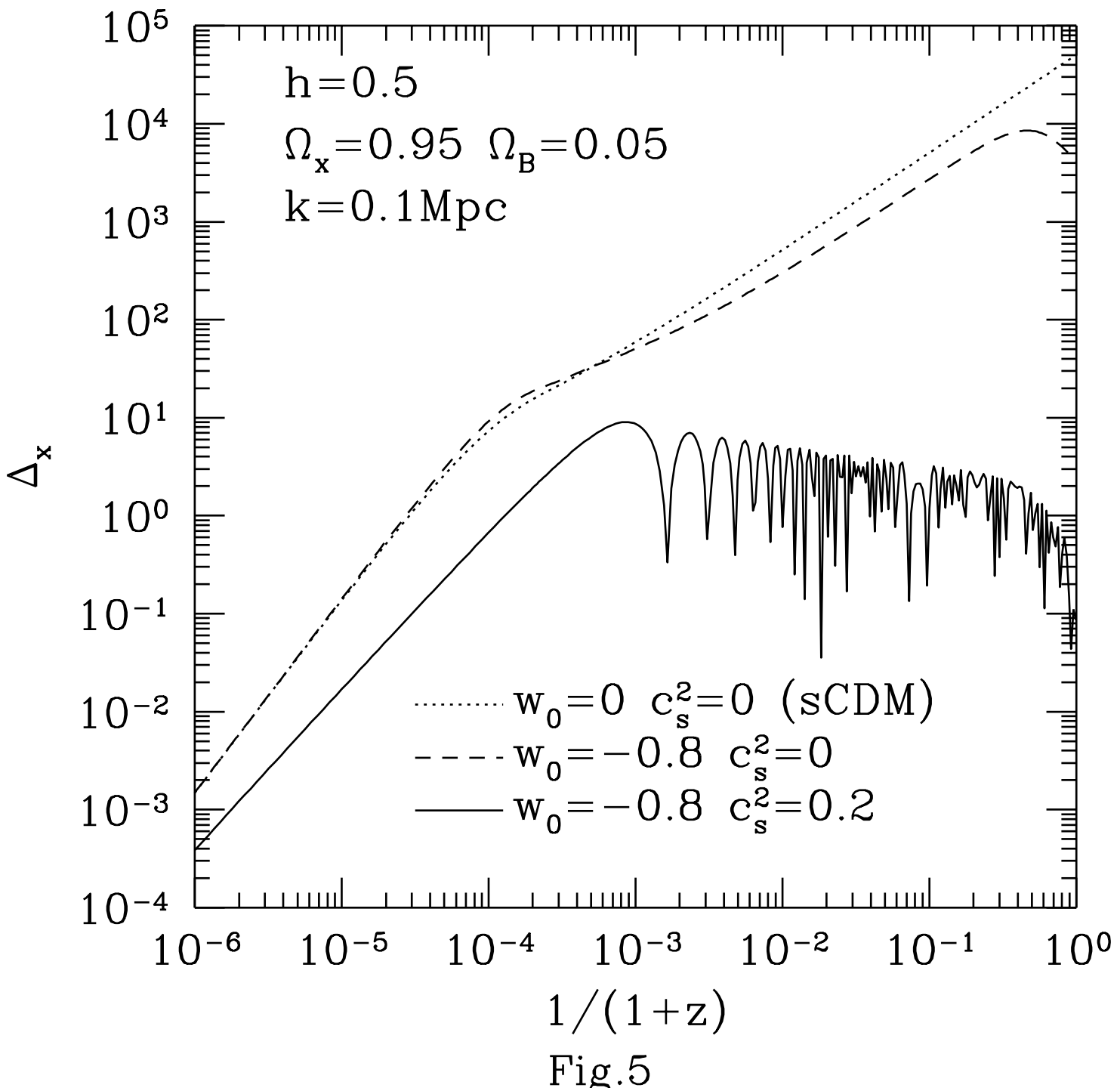


Fig. 4



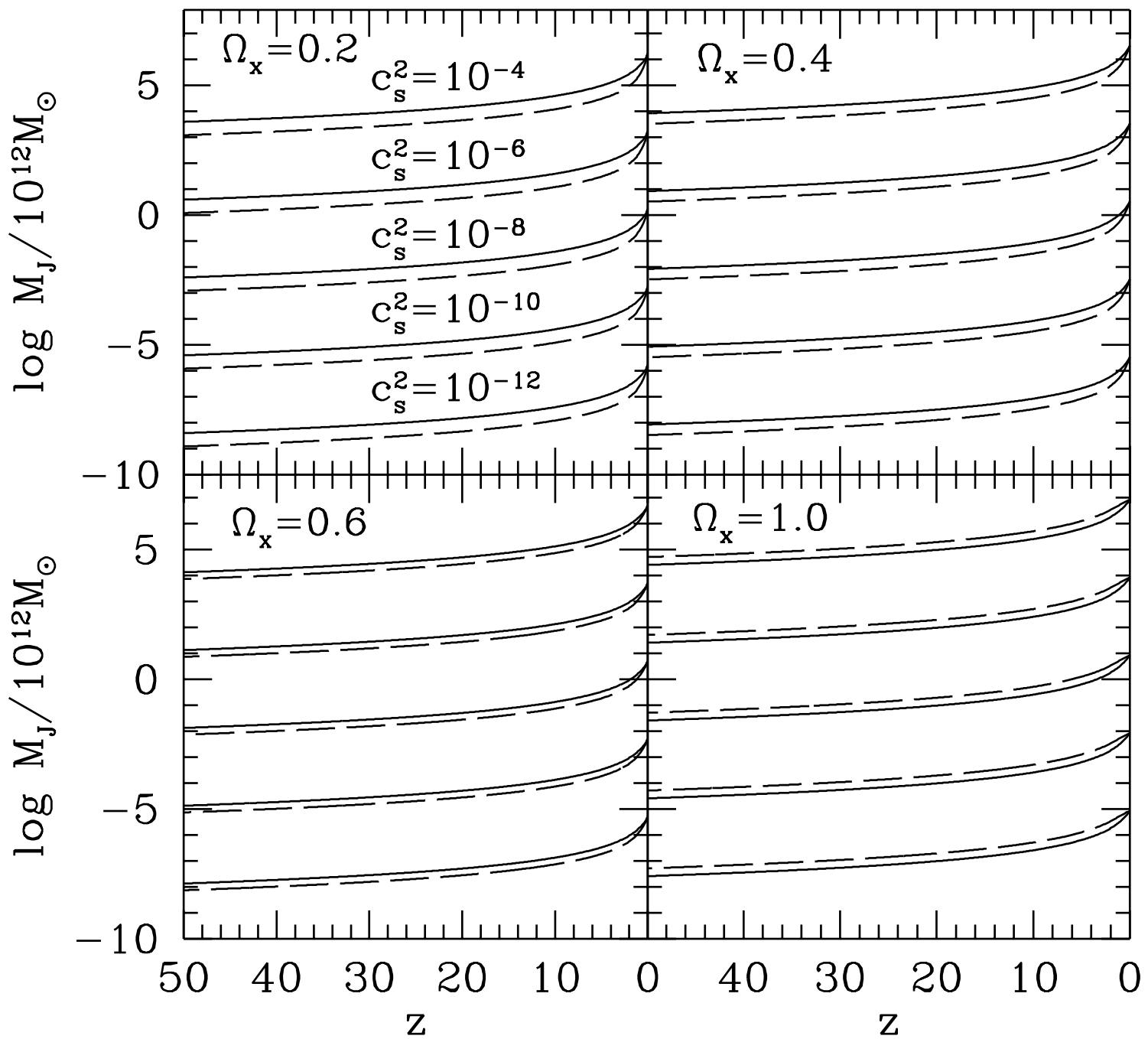


Fig.6

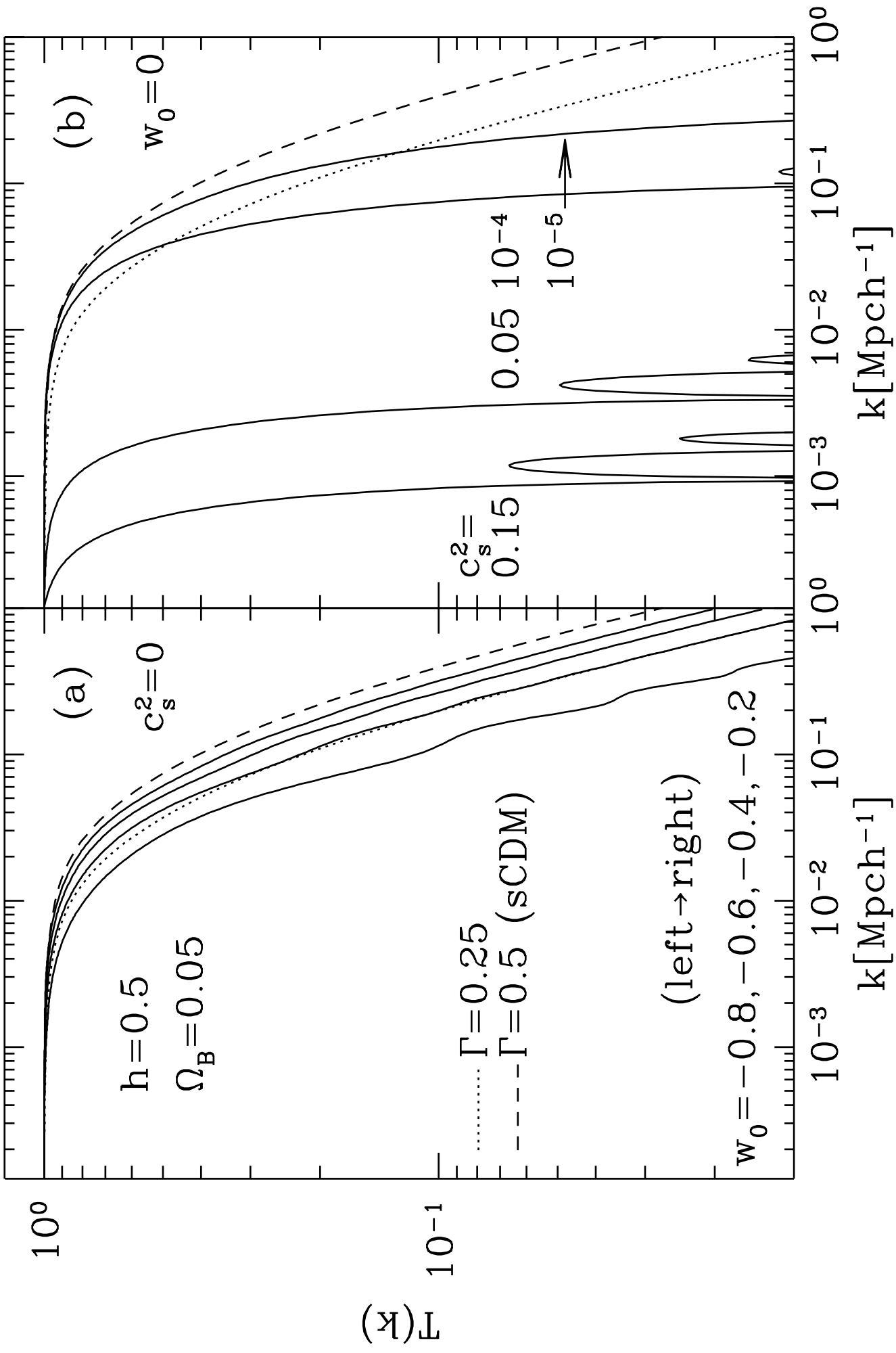


Fig. 7

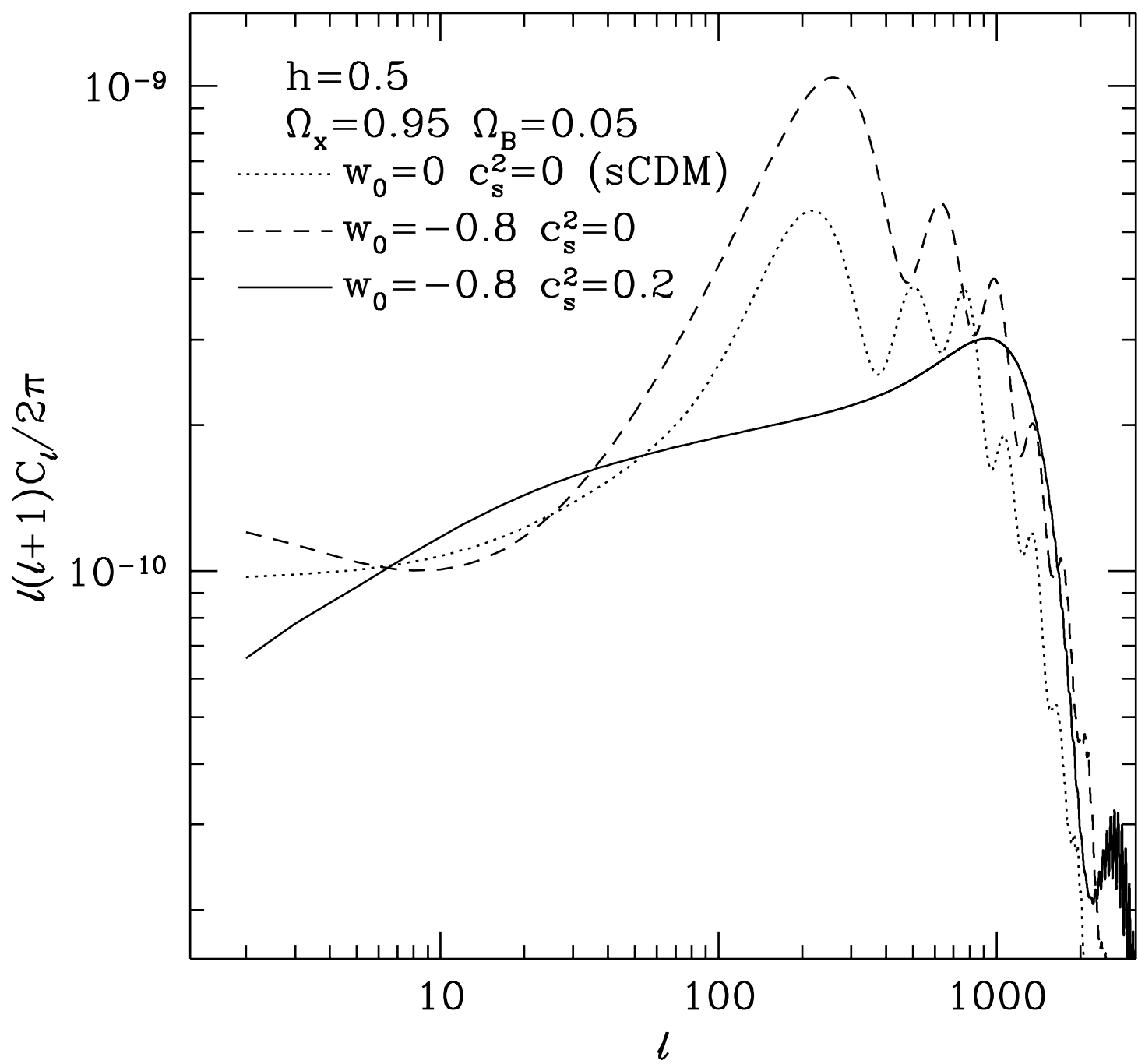


Fig.8

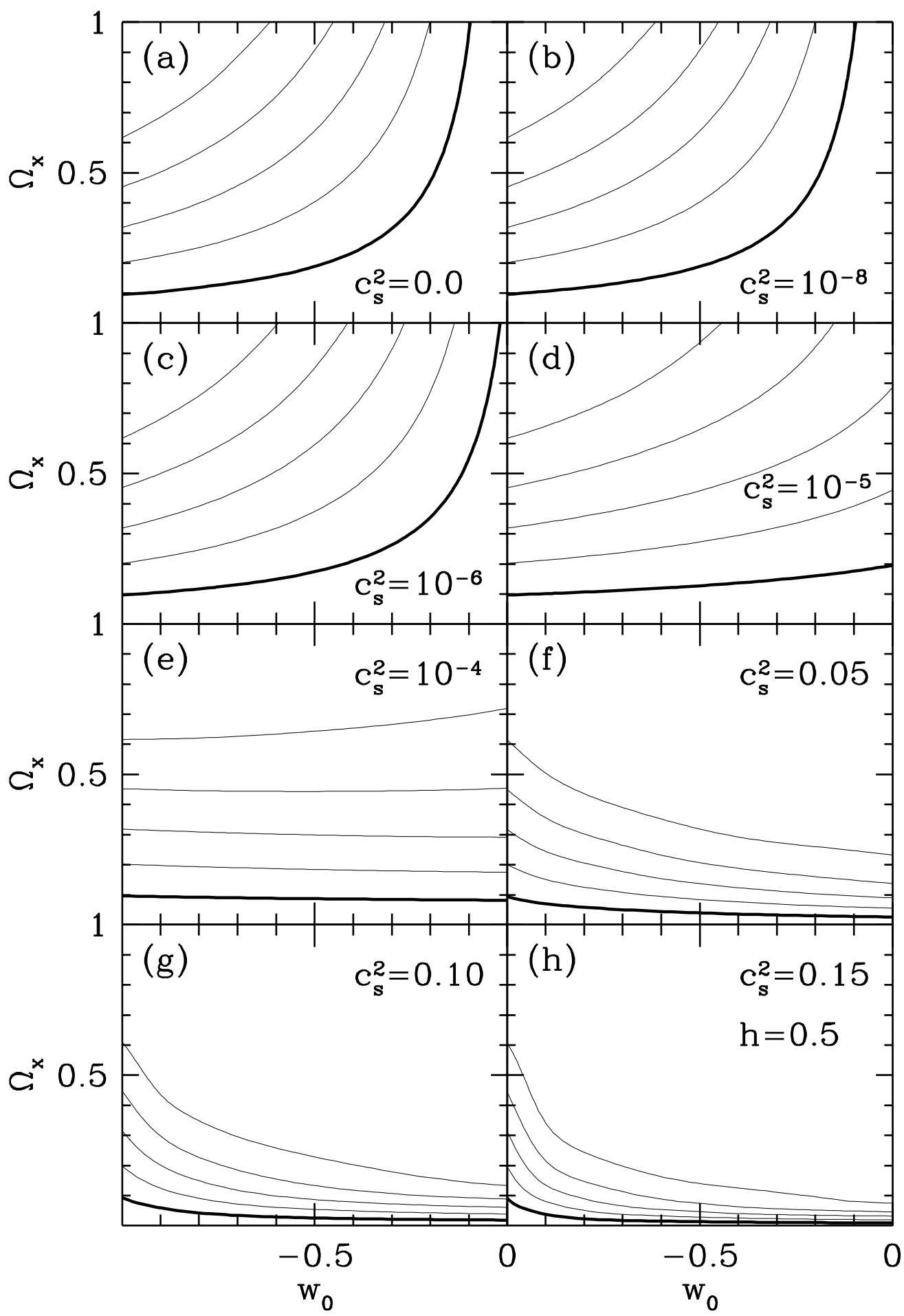


Fig.9

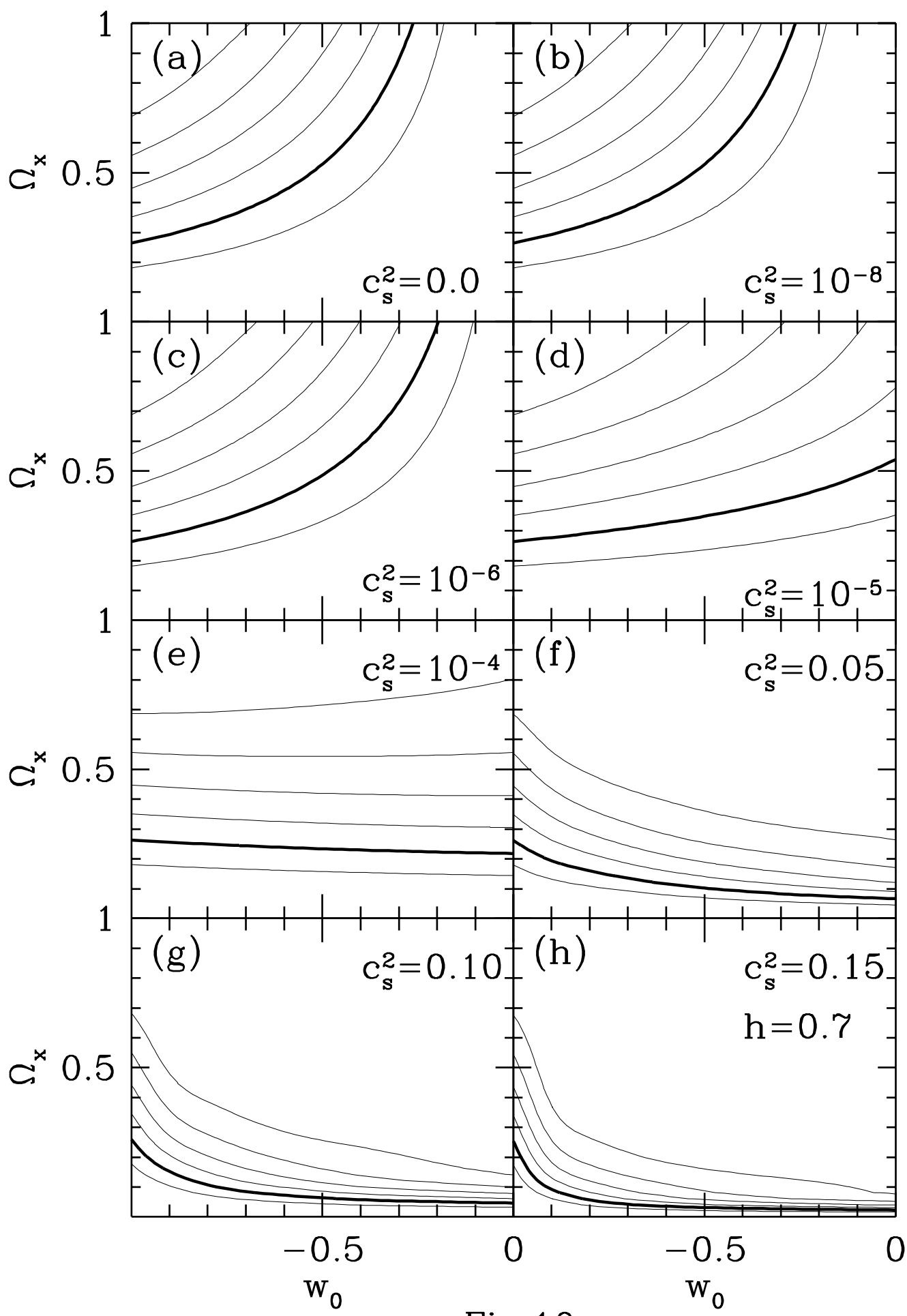


Fig.10

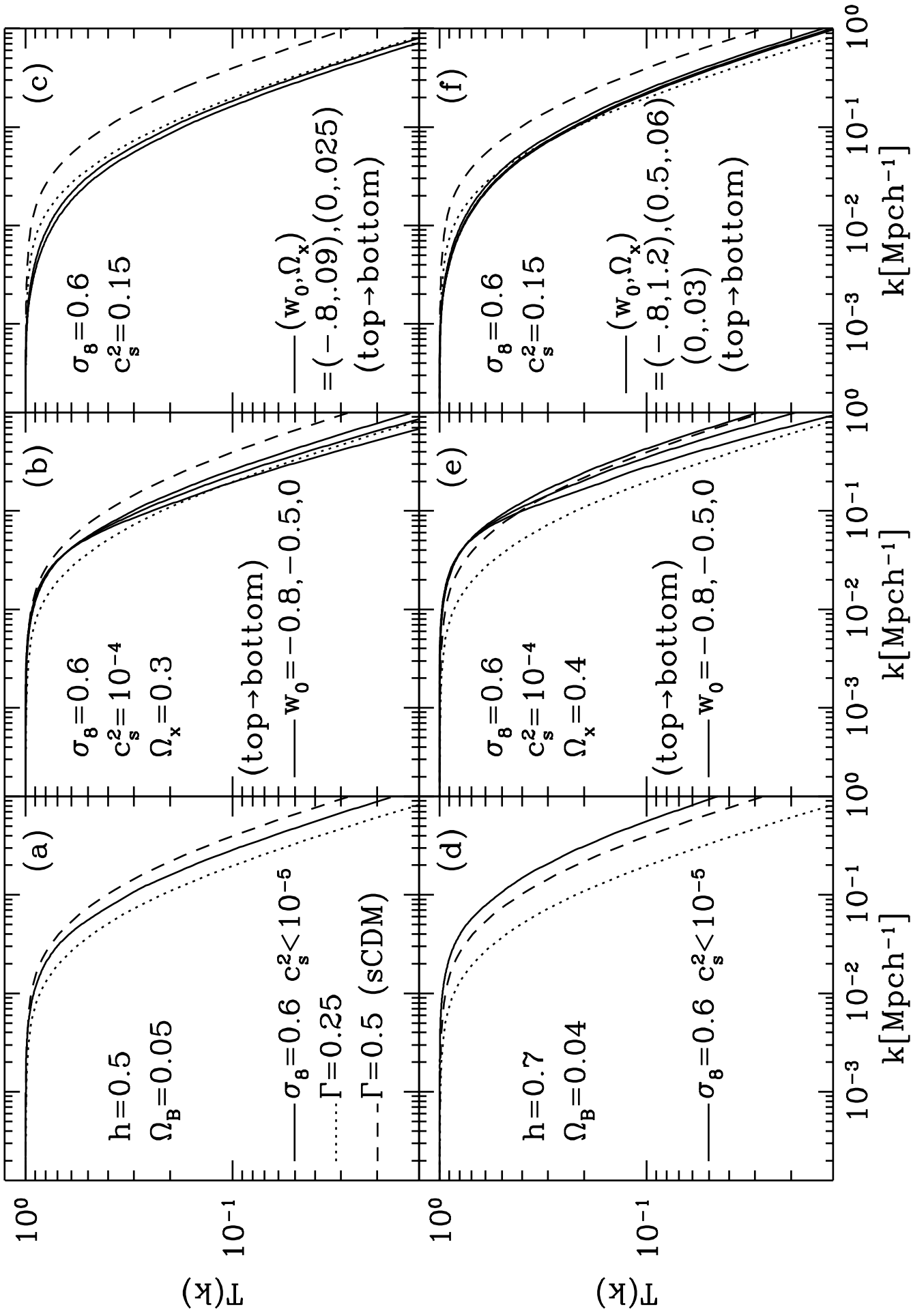


Fig. 11

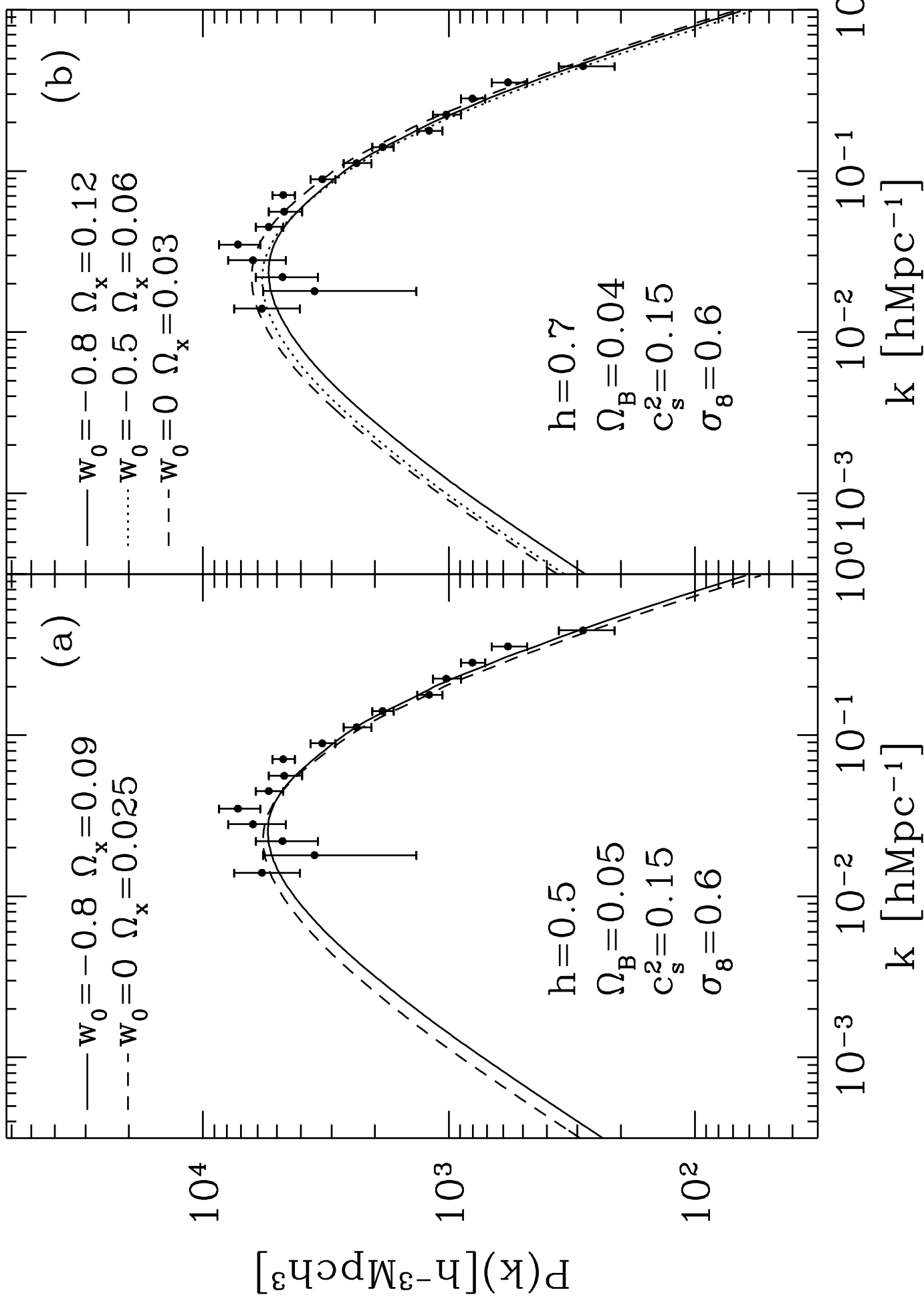


Fig. 12

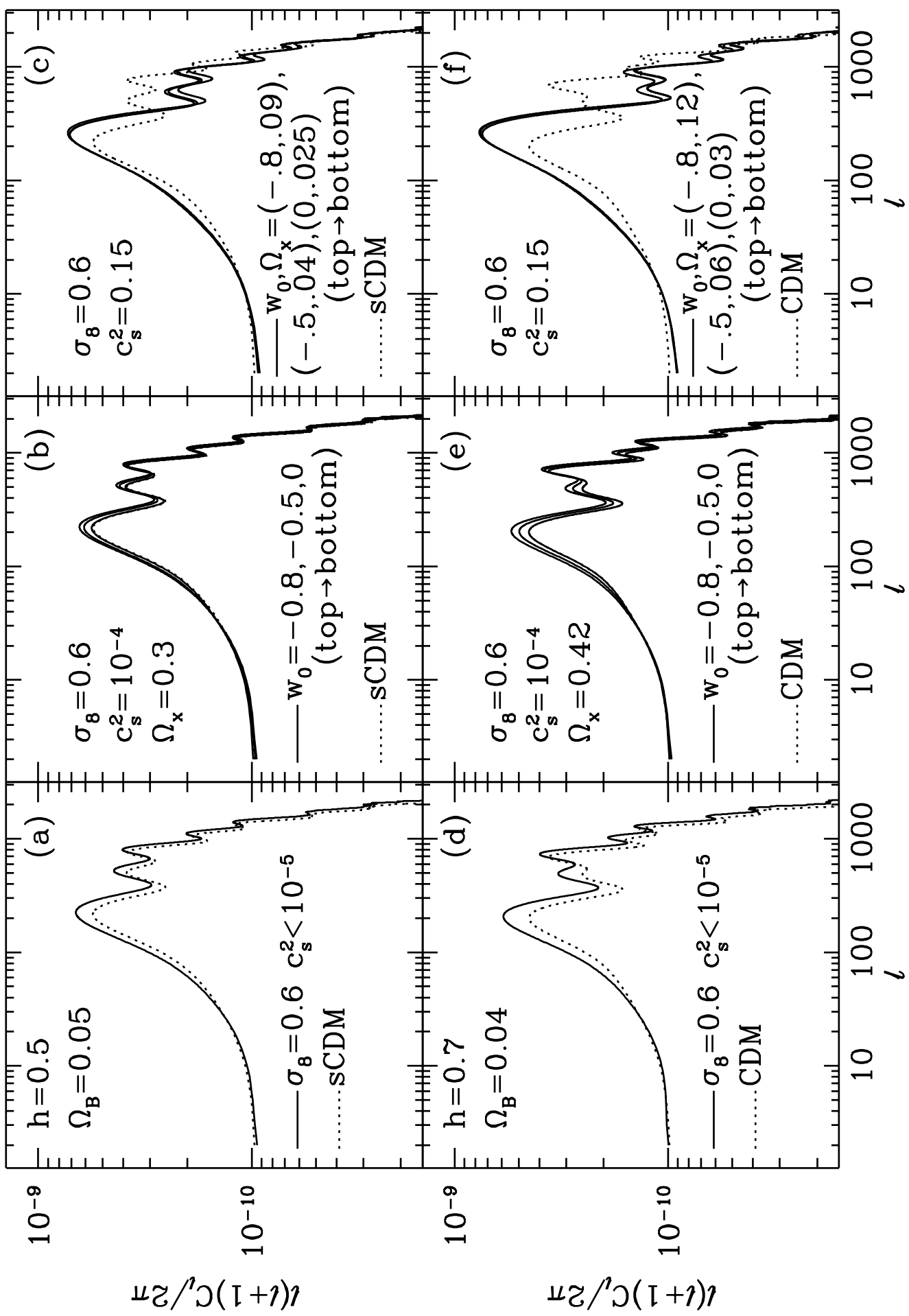


Fig. 13

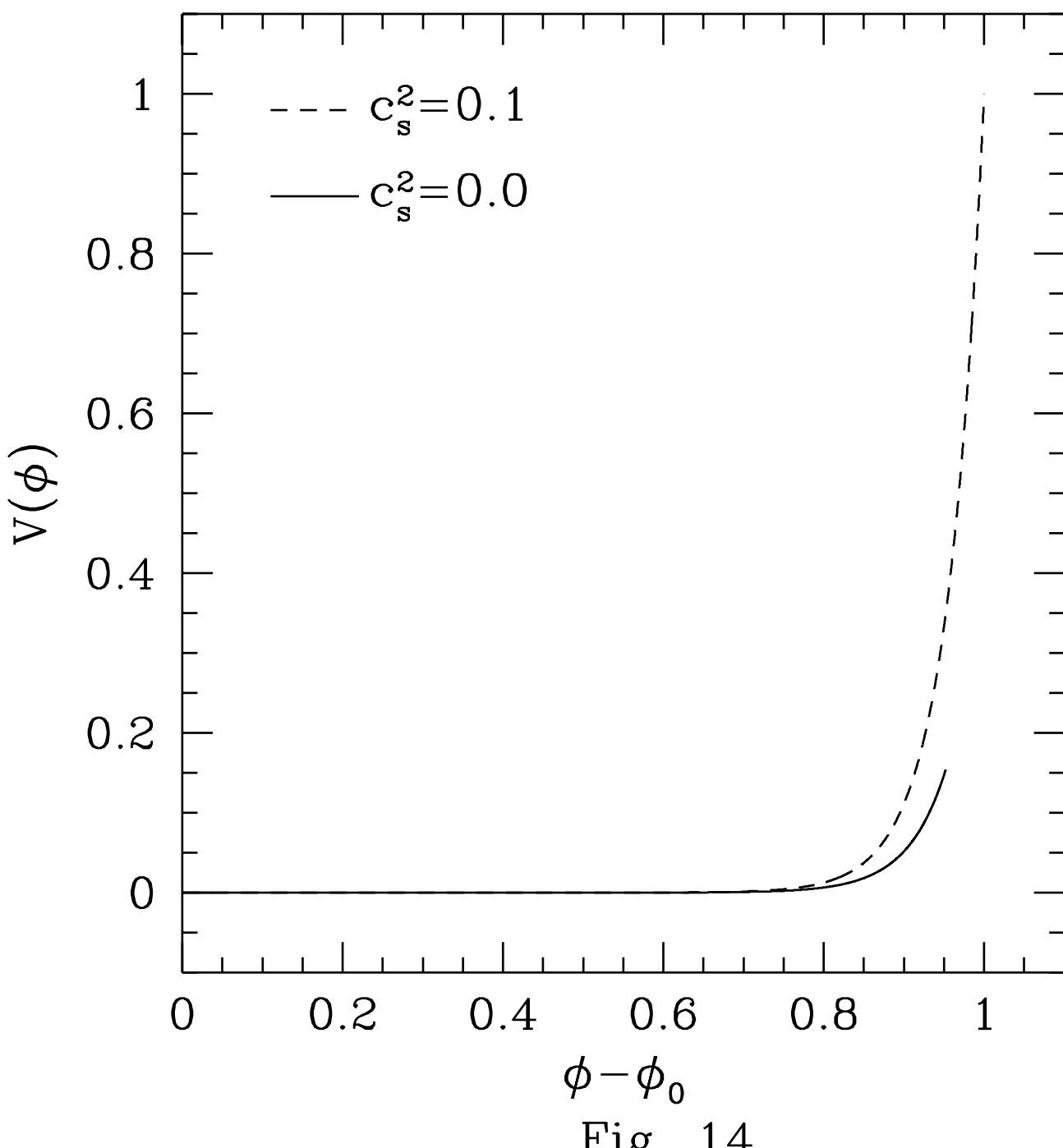


Fig. 14